HELICOPTER ROTOR PERFORMANCE IMPROVEMENT BY PIECEWISE DYNAMIC BLADE TWIST

Yuhang Zhang, zhangyuhang@nuaa.edu.cn, College of Aerospace Engineering, Nanjing University of Aeronautics and Astronautics, Nanjing 210016, China

Dong Han, donghan@nuaa.edu.cn, College of Aerospace Engineering, Nanjing University of Aeronautics and Astronautics, Nanjing 210016, China

Abstract

Piecewise dynamic twist is studied as a method for reducing rotor power and improving rotor performance. A rotor performance calculation model is established based on the anisotropic composite moderate deformation beam model and used to power prediction and flow field analysis at different flight speeds. The theoretical prediction is consistent with the flight test data, which verifies the validity of the analysis model. The blade is divided into inner and outer segments in the radius direction according to the airfoil distribution of UH-60 helicopter. The effect and its mechanism of the piecewise dynamic twist on the rotor power is investigated from the point of view of the angle of attack and lift-to-drag ratio distribution over the disk. Overall, the effect is proportional to the amplitude of the dynamic twist, changes periodically with the phase angle, and increases first and then decreases with the flight speed. A set of piecewise dynamic blade twist schemes are obtained by the traversal method, which are better than the linear negative twist scheme at any flight speed.

1. INTRODUCTION

Helicopters have extensive and irreplaceable applications in military and civilian fields due to their excellent low-altitude and low-speed performance. As the rotor is the main aerodynamic component of a helicopter, how to improve its performance has always been an important topic in the field of helicopter research.

One of the easiest and most widely used methods is to provide the blade section with a pre-twist angle. Through the negative twist of the blades, the aerodynamic environment becomes better and the rotor performance can be improved [1-3]. However, no matter linear twist or advanced nonlinear twist cannot adapt to the diversity of flight states or the periodicity of azimuth angle. Hence a dynamic blade twist that can control the pitch angle actively according to the flight speed and the azimuth angle is needed to further improve the rotor performance.

Although most of studies on dynamic blade twist focused on its effect on noise and vibration reduction [4-9], and the number of studies focused on rotor performance is less relatively. The dynamic twist shows a great potential in improving the rotor performance and reducing the rotor power. Zhang et al. [10] used a weak fluid-structure coupling method to study the benefit of an active rotor, which resulted in a power reduction of about 14%. Wilkie, Park, and Belvin [11] investigated the dynamic stall suppression possible with an active fiber composite rotor blade. The results of the analytical study indicated that the maximum dynamic stall limited rotor thrust and forward speed can be increased by approximately 5% and 10%, respectively, through the use of active blade twist. Han el al. [12] suggested that the rotor power reduction caused by dynamic twist was small in hover and low speed forward speed and became pronounced in high speed It is found that lower harmonic blade twist can achieve larger power savings than higher harmonic twist. The zero harmonic twist dominates the power reductions. D. Douglas Boyd, Jr. [13] predicted an active twist rotor performance by a computational fluid dynamics code, found that the lift-to-drag ratio will reduce due to an increase in rotor profile power when the dynamic twist is used to reduce noise and vibration loads. Rohit Jain [14] investigated the effect of the dynamic twist on the performance of a UH-60A helicopter in high-speed forward flight by a coupled computational fluid dynamic and computational structural dynamics simulation. By applying the dynamic twist on the advancing side, the power reduction was about 3.3%.

Besides, past studies mainly focused on the linear dynamic twist. In view of the application of

advanced nonlinear static twist in improving rotor performance [15-17], piecewise dynamic twist is introduced into the active twist rotor concept to further improve the rotor performance.

In this work, the blade twist is piecewise linear in the spanwise direction. The effect of its amplitude and phase angle on the rotor power and the aerodynamic environment over the disk is investigated. Through a parametric sweep analysis, an optimal piecewise dynamic twist scheme is found to minimize the rotor power. Since the low-order dynamic twist has a greater impact on the rotor power, only the first-order dynamic twist is considered in this paper.

2. FLIGHT PERFORMANCE MODEL

A flight performance model including moderate deformation beam blade structure model, nonlinear quasi-steady aerodynamic model, Pitt-Peters inflow model and trim model is established and used to analyze the rotor performance.

2.1. Blade Stucture Model

A blade structure model based on anisotropic composite moderate deformation beam is established in this part.

2.1.1. Strain-displacement relationship

The position vector of any point on the blade section in the blade coordinate system is expressed as

$$\boldsymbol{r} = \begin{Bmatrix} x \\ 0 \\ 0 \end{Bmatrix} + \boldsymbol{X}_{-\theta} \begin{Bmatrix} 0 \\ \eta \\ \zeta \end{Bmatrix}, \tag{1}$$

where, $\boldsymbol{r}$ is the radius coordinate, η is the chord coordinate of the section, ζ is the coordinate of the vertical chord length of the section. The expression of $\boldsymbol{X}_{-\theta}$ is

$$\boldsymbol{X}_{-\theta} = \begin{bmatrix} 1 & 0 & 0 \\ 0 & \cos\theta & -\sin\theta \\ 0 & \sin\theta & \cos\theta \end{bmatrix}, \tag{2}$$

where, θ is pre-twist angle of the section.

After deformation, the position of the point is

$$\boldsymbol{R} = \begin{Bmatrix} x+u \\ v \\ w \end{Bmatrix} + \boldsymbol{C} \begin{Bmatrix} 0 \\ \eta \\ \zeta \end{Bmatrix} + \boldsymbol{C} \begin{Bmatrix} W_1 \\ W_2 \\ W_3 \end{Bmatrix}, \tag{3}$$

where, u, v and w are the displacements of the intersection of the section and the elastic axis along the x, y and z axis directions, respectively, W_1, W_2 and W_3 are the warping of the three directions respectively, C is the transformation matrix between before and after deformation. According to the classic moderate deformation beam model [18],

$$\boldsymbol{C} = \begin{bmatrix} 1-\frac{v'^2}{2}-\frac{w'^2}{2} & -v'\cos\bar{\theta} - w'\sin\bar{\theta} & v'\sin\bar{\theta} - w'\cos\bar{\theta} \\ v' & (1-\frac{v'^2}{2})\cos\bar{\theta} & (1-\frac{w'^2}{2})\sin\bar{\theta} \\ w' & -(1-\frac{v'^2}{2})\sin\bar{\theta} & (1-\frac{w'^2}{2})\cos\bar{\theta} \end{bmatrix}, \tag{4}$$

where, $\bar{\theta} = \theta + \phi - \int_0^x w'v''\,\mathrm{d}x$, ϕ is the twist angle around the elastic axis.

According to the nonlinear composite beam theory [19], the moment strain of the beam can be expressed as

$$\boldsymbol{\kappa} = \boldsymbol{K} - \boldsymbol{k}, \tag{5}$$

where, $\boldsymbol{k}$ and $\boldsymbol{K}$ are the curvature vector of the beam before and after the deformation. And

$$\widetilde{\boldsymbol{K}} = \boldsymbol{C}^{\mathrm{T}}\boldsymbol{C}', \tag{6}$$

$$\widetilde{\boldsymbol{k}} = (\boldsymbol{X}_{-\theta})^{\mathrm{T}}(\boldsymbol{X}_{-\theta})', \tag{7}$$

among them, the operator "~" represents the following operation rules

$$\begin{Bmatrix} \widetilde{x} \\ y \\ z \end{Bmatrix} = \begin{bmatrix} 0 & -z & y \\ z & 0 & -x \\ -y & x & 0 \end{bmatrix}. \tag{8}$$

Substitute equation (2), equation (4), equation (6) and equation (7) into equation (5), we get

$$\boldsymbol{\kappa} = \begin{Bmatrix} \phi' \\ -\cos\bar{\theta}w'' + \sin\bar{\theta}v'' \\ \sin\bar{\theta}w'' + \cos\bar{\theta}v'' \end{Bmatrix}. \tag{9}$$

Force strain is expressed as

$$\boldsymbol{\gamma} = \boldsymbol{C}^{\mathrm{T}} \begin{Bmatrix} 1+u' \\ v' \\ w' \end{Bmatrix} - \begin{Bmatrix} 1 \\ 0 \\ 0 \end{Bmatrix} = \begin{Bmatrix} \bar{\varepsilon}_{11} \\ 2\bar{\varepsilon}_{12} \\ 2\bar{\varepsilon}_{13} \end{Bmatrix}. \tag{10}$$

Substitute equation (4) into equation (10), we get

$$\boldsymbol{\gamma} = \begin{Bmatrix} u_{\mathrm{e}}' \\ 0 \\ 0 \end{Bmatrix}, \tag{11}$$

where,

$$u_{\mathrm{e}}' = u' + \frac{v'}{2} + \frac{w'}{2}. \tag{12}$$

2.1.2. Beam strain energy

In blade dynamics, the influence of shear force and external stress of a section is usually ignored, so the beam section force and moment have the following relationship with strain

$$\begin{Bmatrix} F_x \\ M_x \\ M_y \\ M_z \end{Bmatrix} = \int \boldsymbol{T} \begin{Bmatrix} \sigma_{11} \\ \sigma_{12} \\ \sigma_{13} \end{Bmatrix} \mathrm{d}A \tag{13}$$

and

(14) $\boldsymbol{T}=\begin{bmatrix} 1 & 0 & 0 \\ -\theta'(\zeta\lambda_\eta-\eta\lambda_\zeta)+\phi'(\eta^2+\zeta^2) & \lambda_\eta-\zeta & \lambda_\zeta+\eta \\ \zeta & 0 & 0 \\ -\eta & 0 & 0 \end{bmatrix}$,

where, λ is the warpage function. We have

(15) $\begin{Bmatrix}\sigma_{11}\\ \sigma_{12}\\ \sigma_{13}\end{Bmatrix}=\begin{bmatrix}Q_{11} & Q_{15} & Q_{16}\\ Q_{51} & Q_{55} & Q_{56}\\ Q_{61} & Q_{65} & Q_{66}\end{bmatrix}\begin{Bmatrix}\varepsilon_{11}\\ 2\varepsilon_{12}\\ 2\varepsilon_{13}\end{Bmatrix}$

and

(16) $\begin{Bmatrix}\varepsilon_{11}\\ 2\varepsilon_{12}\\ 2\varepsilon_{13}\end{Bmatrix}=\boldsymbol{T}^{\mathrm{T}}\begin{Bmatrix}u'_{\mathrm{e}}\\ \phi'\\ \kappa_y\\ \kappa_z\end{Bmatrix}$,

where, the coefficient in equation (15) is determined by the blade material.

Substitute equation (14) – (16) into Equation (13), the constitutive relationship can be expressed as

(17) $\begin{Bmatrix}F_x\\ M_x\\ M_y\\ M_z\end{Bmatrix}=\boldsymbol{S}_{4\times4}\begin{Bmatrix}u'_{\mathrm{e}}\\ \phi'\\ \kappa_y\\ \kappa_z\end{Bmatrix}$,

where, $\boldsymbol{S}_{4\times4}$ is the stiffness matrix, which can be expressed as

(18) $\boldsymbol{S}_{4\times4}=\begin{bmatrix} S_{uu} & S_{u\phi}+\frac{1}{2}\phi' S_{uu}k_p^2 & S_{uw} & S_{uv} \\ S_{\phi u}+\phi' S_{uu}k_p^2 & S_{\phi\phi} & S_{\phi w} & S_{\phi v} \\ S_{wu} & S_{w\phi} & S_{ww} & S_{wv} \\ S_{vu} & S_{v\phi} & S_{vw} & S_{vv} \end{bmatrix}$.

The strain energy of the beam can be expressed in the form of the section force, namely

(19) $\delta U=\int(\delta\varepsilon)^{\mathrm{T}}\sigma\mathrm{d}V$
$=\int_0^R[F_x\delta u'_e+M_x\delta\phi'+M_y\delta\kappa_y+M_z\delta\kappa_z]\mathrm{d}r.$

From the elastic potential energy variational expression, the elastic generalized forces caused by the elastic potential energy can be separated, and then the stiffness matrix can be obtained by

(20) $K_{\mathrm{ij}}^{\mathrm{E}}=\frac{\partial Q_i^{\mathrm{E}}}{\partial q_j}$.

2.2. Kinetic Energy

When describing the motion of the blade, the influence of structural warpage is ignored, the variation of the blade kinetic energy can be expressed as

(21) $\delta\boldsymbol{T}=\sum_{i=1}^n Q_i^{\mathrm{T}}\delta q_i=\sum_{i=1}^n\int_0^{\mathrm{R}}\iint_A-\rho\ddot{\boldsymbol{R}}\frac{\partial\boldsymbol{R}}{\partial q_i}\mathrm{d}A\mathrm{d}r\,\delta q_i$,

where, ρ is air density, Q_i^{T} is the generalized force caused by kinetic energy. Hence, the generalized force produced by kinetic energy is

(22) $\int_0^{\mathrm{R}}\iint_A-\rho\ddot{\boldsymbol{R}}\frac{\partial\boldsymbol{R}}{\partial q_i}\mathrm{d}A\mathrm{d}r$,

According to analytical mechanics, the tangent mass matrix, damping matrix and stiffness matrix are

(23) $M_{ij}^{\mathrm{T}}=\frac{\partial Q_i^{\mathrm{T}}}{\partial\ddot{q}_j}=-\int_0^{\mathrm{R}}\iint_A\rho\frac{\partial\boldsymbol{R}}{\partial q_j}\cdot\frac{\partial\boldsymbol{R}}{\partial q_i}\mathrm{d}A\mathrm{d}r$,

(24) $C_{ij}^{\mathrm{T}}=\frac{\partial Q_i^{\mathrm{T}}}{\partial\dot{q}_j}=-\int_0^{R}\iint_A 2\rho\frac{\partial\dot{\mathbf{R}}}{\partial q_j}\cdot\frac{\partial\mathbf{R}}{\partial q_i}\mathrm{d}A\,\mathrm{d}L$,

and

(25) $K_{ij}^{\mathrm{T}}=\frac{\partial Q_i^{\mathrm{T}}}{\partial q_j}=-\int_0^{R}\iint_A\rho\left(\frac{\partial\ddot{\mathbf{R}}}{\partial q_j}\cdot\frac{\partial\mathbf{R}}{\partial q_i}+\ddot{\mathbf{R}}\cdot\frac{\partial^2\mathbf{R}}{\partial q_i\partial q_j}\right)\mathrm{d}A\,\mathrm{d}L$.

2.3. Aerodynamic Model

In this model, in order to calculate the aerodynamic force consistently, calculate the velocity of any point on the blade pitch axis in the inertial coordinate system, project the blade plane to the inertial coordinate system, and calculate the pitch axis of the blade, successively. The local airflow velocity is obtained by converted into the deformed coordinate system. According to the nonlinear quasi-steady aerodynamic model, the air velocity and angle of attack on the blade profile can be calculated. Then get the aerodynamic force of the blade profile, including lift, drag and pitch moment through the look-up table method. Finally, the virtual work generated by the above aerodynamic force is calculated, and the generalized aerodynamic force and its derived tangent damping matrix and stiffness matrix are given.

The resultant aerodynamic force and moment of the airfoil section are converted to the inertial coordinate system, and the variation of the work generated by the aerodynamic force can be obtained. The expression is

(26) $\delta W^{\mathrm{A}}=\sum_{i=1}^n Q_i^{\mathrm{A}}\delta q_i=\int_0^R(\boldsymbol{F}_{\mathrm{A}}\cdot\delta\boldsymbol{R}+\boldsymbol{M}_{\mathrm{A}}\cdot\delta\boldsymbol{a})\mathrm{d}r$,

where, $\boldsymbol{F}_{\mathrm{A}}$ is the aerodynamic force; $\boldsymbol{R}$ is the position vector; $\boldsymbol{M}_{\mathrm{A}}$ is the aerodynamic moment; $\boldsymbol{a}$ is the angle vector. Therefore, the generalized force generated by aerodynamic force is

(27) $Q_i^{\mathrm{A}}=\int_0^R\left(\boldsymbol{F}_{\mathrm{A}}\cdot\frac{\partial\boldsymbol{R}}{\partial q_i}+\boldsymbol{M}_{\mathrm{A}}\cdot\frac{\partial\boldsymbol{a}}{\partial q_i}\right)\mathrm{d}r$.

2.4. Inflow Model

The induced velocity distribution used in this model is calculated according to the Pitt-Peters inflow model [20]. According to the model, the

induced velocity in the rotor plane changes along the span and azimuth, and the distribution law is

$$(28)\ \lambda(r,\psi) = \lambda_0 + \frac{r}{R}(\lambda_{1c}\cos\psi + \lambda_{1s}\sin\psi),$$

where, λ_0 is the static component, λ_{1c} is the first-order cosine component, and λ_{1s} is the first-order sine component.

2.5. Blade Dynamics Equations

The implicit nonlinear dynamic equation in the form of generalized force includes four terms: elastic potential energy term, kinetic energy term, and aerodynamic force term. Therefore, the system motion equation can be rewritten as

$$(29)\ Q_i^{\mathrm{E}} + Q_i^{\mathrm{T}} + Q_i^{\mathrm{A}} = 0\ \ (i = 1,2,\cdots,n).$$

In order to ensure the convergence and accuracy of the numerical calculations, the implicit differential equation is solved by using the Newmark numerical integration method [21]

2.6. Trim Model

In any constant flying state, the helicopter trim equation set under the assumption of a small angle is

$$(30)\ \begin{cases} W - T_{\mathrm{MR}} = 0 \\ D + H_{\mathrm{MR}} - T_{\mathrm{MR}}\theta_{\mathrm{F}} = 0 \\ Y_{\mathrm{MR}} + T_{\mathrm{TR}} + T_{\mathrm{TR}}\phi_{\mathrm{F}} = 0 \\ M_{y\mathrm{MR}} + M_{y\mathrm{F}} + W(h\theta_{\mathrm{F}} - x_{\mathrm{cg}}) = 0 \\ M_{x\mathrm{MR}} + M_{x\mathrm{F}} + W(h\phi_{\mathrm{F}} - y_{\mathrm{cg}}) + T_{\mathrm{TR}}h_{\mathrm{TR}} = 0 \\ Q_{\mathrm{MR}} - T_{\mathrm{TR}}l_{\mathrm{TR}} = 0 \end{cases}$$

where, W is the helicopter gravity, D is the fuselage resistance, T_{MR} is the rotor pull, H_{MR} is the rotor backward force, Y_{MR} is the rotor lateral force, T_{TR} is the tail rotor pull, $M_{x\mathrm{MR}}$ is the rotor roll moment, $M_{y\mathrm{MR}}$ is the rotor pitch moment, Q_{MR} is the reverse torque, $M_{x\mathrm{F}}$ The fuselage rolling moment, $M_{y\mathrm{F}}$ is the fuselage pitch moment, h is the distance between the rotor hub and the helicopter's center of gravity in the z-axial direction, h_{TR} is the distance between the rotor hub and the tail rotor hub in the z-axial direction, l_{TR} is the tail rotor hub and the helicopter's center of gravity on the x-axis The distance of the direction, x_{cg} is the distance between the center of gravity of the helicopter and the axis, y_{cg} is the distance between the center of gravity of the helicopter and the axis, θ_{F} is the pitch angle of the fuselage, ϕ_{F} is the roll angle of the fuselage.

When the aero-elastic response of the rotor converges, the obtained rotor hub force and torque are substituted into the balance equation to solve for the rotor control and the attitude angle of the body, and the obtained value is used to recalculate the aero-elastic response of the rotor until the rotor response When the sum trim variable converges, the steady-state response of the rotor can be obtained, and then the required power of the rotor can be obtained.

2.7. Model Validation

The flight data of the UH-60 helicopter [22] is utilized to validate the rotor model used in this work. The comparisons between the predictions of the rotor power and the flight test data with the takeoff weight coefficient of 0.0065 and 0.0074 are shown in Figure 1, and the predictions by the present method are generally in good agreement with the flight test data for the cases considered.

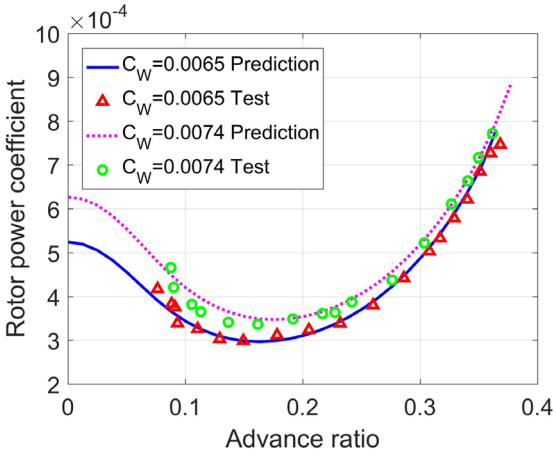

Figure 1 Comparison of predictions with flight test data.

3. PIECEWISE BLADE DYNAMIC TWIST

Piecewise blade dynamic twist means the twist angle varies at different azimuth angles, and the angle is a piecewise function of the dimensionless radius coordinate.

For a UH-60 helicopter, its blade is divided into three segments according to airfoil distribution, as shown in Figure 2. Ignore the tip segment because of its small length, the blade can be seen as divided into two segments, called inner segment and outer segment respectively. And the dimensionless radius coordinate of the segment point is 0.5. Note that the tip sweep is not considered in this work.

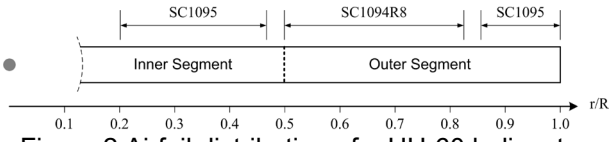

Figure 2 Airfoil distribution of a UH-60 helicopter blade

For a point whose radius coordinate is r/R, local pitch angle can be expressed as

(31) $\theta = \theta_0 + \theta_{1c}\cos\psi + \theta_{1s}\sin\psi + \theta_{pre} + \theta_{dt}$,

where, θ_0 is collective pitch angle, θ_{1c} is lateral pitch angle, θ_{1s} is longitudinal pitch angle, θ_{pre} is pre-twist angle, and θ_{dt} is dynamic twist angle which can be expressed as

(32) $$\theta_{dt} = \begin{cases} \frac{r}{R}\theta_{dt}^{in}\cos\left(N^{in}\psi + \phi_{dt}^{in}\right) & 0 \le \frac{r}{R} < 0.5 \\ \left(\frac{r}{R}\theta_{dt}^{out} + \theta_{dt}^{0}\right)\cos(N^{out}\psi + \phi_{dt}^{out}) & 0.5 \le \frac{r}{R} < 1 \end{cases},$$

where, ψ is the azimuth angle, θ_{dt}^{in} and θ_{dt}^{out} are the amplitudes of the dynamic twist applied on the two segments, N^{in} and N^{out} are the orders of the dynamic twist applied on the two segments, ϕ_{dt}^{in} and ϕ_{dt}^{out} are the phase angle of the dynamic twist applied on the two segments, and θ_{dt}^{0} is a parameter to keep the twist angle continuous along the blade.

In previous studies, the first-order linear dynamic twist shows a great influence to reduce rotor. So in this paper, the effect of the first-order piecewise dynamic twist is focused on, which means

(33) $N^{in} = N^{out} = 1$,

and then the expression of θ_{dt}^{0} is

(34) $$\theta_{dt}^{0} = \frac{1}{2}\left(\frac{\cos\left(\psi+\phi_{dt}^{in}\right)}{\cos\left(\psi+\phi_{dt}^{out}\right)}\theta_{dt}^{in} - \theta_{dt}^{out}\right).$$

Substitute equation (33) and (34) into equation (32), the expression of θ_{dt} becomes

(35) $$\theta_{dt} = \begin{cases} \frac{r}{R}\theta_{dt}^{in}\cos\left(\psi+\phi_{dt}^{in}\right) & 0 \le \frac{r}{R} < 0.5 \\ \left(\frac{r}{R}-\frac{1}{2}\right)\theta_{dt}^{out}\cos\left(\psi+\phi_{dt}^{out}\right) + \frac{1}{2}\theta_{dt}^{in}\cos\left(\psi+\phi_{dt}^{in}\right) & 0.5 \le \frac{r}{R} < 1 \end{cases}.$$

4. PERFORMANCE ANALYSIS

In this work, the amplitude is limited to less than 5 °/*R* for feasibility considerations, and the dynamic twist is applied on a blade with a 12 °/*R* linear negative static twist. Since the first-order linear dynamic twist has a higher ability to improve the rotor performance, when analyzing the effect of the piecewise linear dynamic twist, the dynamic twist order on each segment is set to one.

4.1. Effect of Outer Segment Dynamic Twist

In this part, the effect of dynamic twist applied on the outer blade on rotor performance is studied. So there is no dynamic twist acts on the inner segment, which means that θ_{dt}^{in} in this part is set to 0.

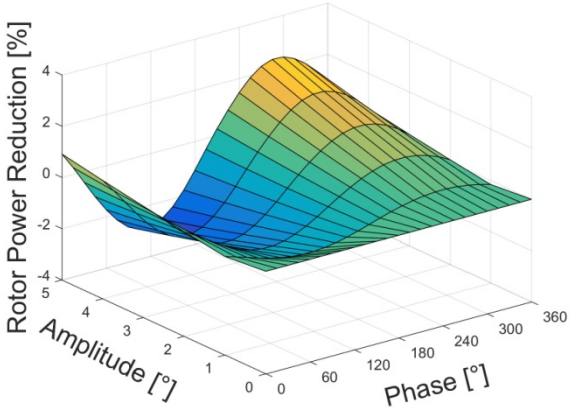

Figure 3 Power reductions with amplitude and phase

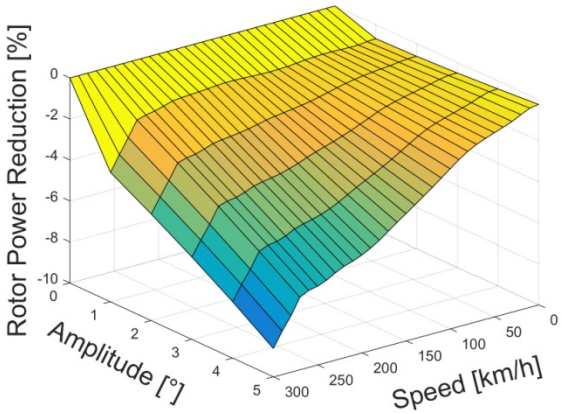

(a) 120° phase angle

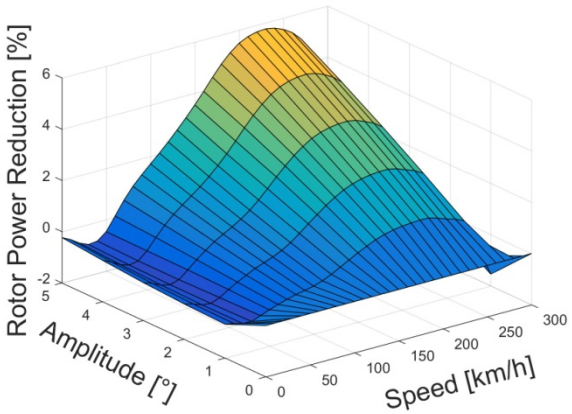

(b) 285° phase angle

Figure 4 Power reductions with amplitude for different speed

4.1.1. View of the rotor power

Figure 3 shows the rotor power reduction while applying dynamic twist with different amplitudes and phase angles at a speed of 120 km/h (closed to cruise speed) on the outer segment. At the speed, the effect of the dynamic twist is approximately proportional to the amplitude and varies periodically with the phase angle. The effect of the dynamic

twist depends on the setting of the phase angle. A 120° phase angle is the least ideal for reducing rotor power, which can lead to a 2% rotor power increase with a 5 °/*R* amplitude. A 285° phase angle seems to be a good choice for reducing power.

Figure 4 shows the rotor power reduction while applying dynamic twist with different amplitudes on the outer segment at different speeds while the phase angle is set as 120° and 285° respectively.

Figure 4(a) verifies the above analysis again that a phase angle of 120° harms the power reduction at any speed, and the negative effect is proportional to flight speed.

When setting an appropriate phase angle, as shown in Figure 4(b), the dynamic twist will reduce power for most flight speeds. When the speed is lower than 230 km/h, the effect is approximately proportional to the speed, and then slightly reduced.

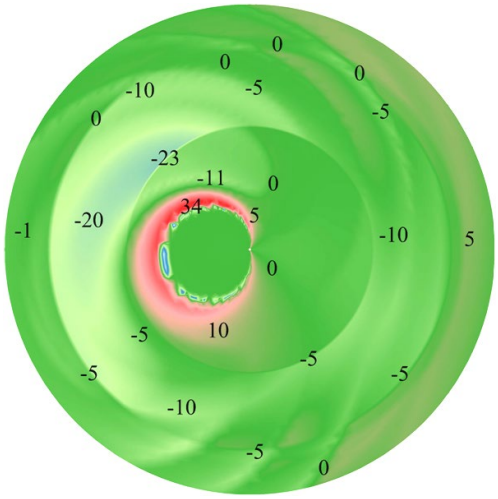

(a) $\theta_{\mathrm{dt}}^{\mathrm{out}} = 2°/R$

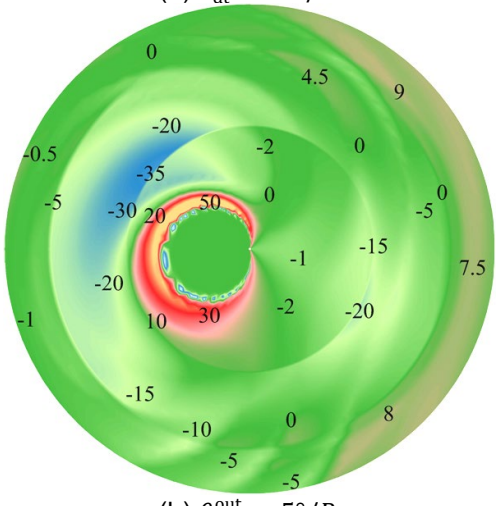

(b) $\theta_{\mathrm{dt}}^{\mathrm{out}} = 5°/R$

Figure 5 L/D difference caused by dynamic twist ($\phi_{\mathrm{dt}}^{\mathrm{out}} = 285°, \mathrm{V} = 230\ \mathrm{km/h}$)

4.1.2. View of AoA and L/D distribution

Figure 5 shows the difference in the L/D over the rotor disk caused by 2 °/*R* and 5 °/*R* amplitude dynamic twists on the outer blade compared with the case without the dynamic twist.

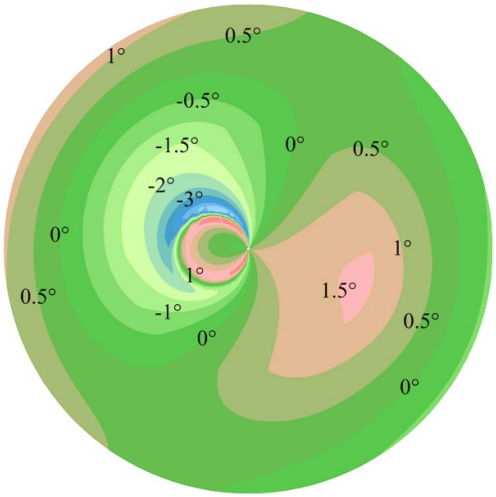

(a) $\phi_{\mathrm{dt}}^{\mathrm{out}} = 120°$

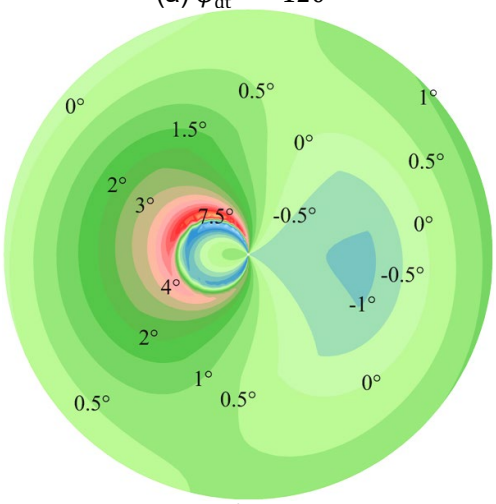

(b) $\phi_{\mathrm{dt}}^{\mathrm{out}} = 285°$

Figure 6 AoA difference caused by dynamic twist ($\theta_{\mathrm{dt}}^{\mathrm{out}} = 5\ °/R, \mathrm{V} = 230\ \mathrm{km/h}$)

The amplitude of the dynamic twist of the outer blade does not change the influence law of dynamic twist on the L/D over the rotor disk, but only changes its value, which explains the reason why the power reduction is proportional to the amplitude. Several obvious features are that the dynamic twist increases the L/D of the advancing blade tip, slightly reduces the value of the retreating blade tip, and causes a large L/D reduction in the middle part of the retreating blade. However, the reduction area is relatively small, and the dynamic twist leads to a reduction in the area of the reverse flow area, resulting in a significant increase in L/D of the area adjacent to the reduction zone on the rotor shaft side, thereby forming a certain compensation.

Therefore, the reduction of the L/D in the area does not have a large negative impact on the rotor power.

Figure 6 shows the difference in the angle of attack (AoA) distribution over the rotor disk caused by dynamic twist with 120° and 285° phase angle on the outer blade compared with the case without the dynamic twist. An intuitive impression is that the two figures seem to be symmetrical to each other if ignoring the reverse flow area. The dynamic twist on the outer blade can increase slightly the AoA at the blade tip and reduce that at the middle of the blade on one side, and make an opposite effect on the other side. And the phase angle of the dynamic twist approximately characterizes the direction of the axis of symmetry. When the phase angle varies from 0° to 360°, the effect will rotate around the rotor shaft with a corresponding angle, which explains the reason that the rotor power reduction varies periodically with the phase angle as shown in Figure 3.

In Figure 6(b), the dynamic twist reduces the AoA at the middle of the advancing blade, which was undergoing a large airflow velocity. Hence the AoA reduction can bring a considerable drag reduction, although a small lift loss occurs. The AoA increase on the retreating side just balances the reduction of lift on the advancing side, and due to the relatively small airflow velocity on this side, the increase does not lead to a big drag increase. The dynamic twist with a 120° phase angle makes an opposite effect and results in a rotor performance reduction.

Figure 7 shows the AoA distribution at different speeds without applying any dynamic twist, namely it is the situation for 12 °/*R* linear negative twist. Figure 8 gives the AoA distribution at corresponding flight speed while applying a dynamic twist with 5 °/*R* amplitude and 285° phase angle.

At the speed of 80 km/h, the dynamic twist does not change the distribution law of the AoA over the rotor disk, but only increases the value at each position by about one to two degrees, thereby improving the rotor performance. At the speed of 230 km/h, the dynamic twist significantly increases AoA in the middle of the retreating blade and reduces that figure in the middle of the advancing blade. For the same reason mentioned in the phase angle analysis, at this speed, the dynamic twist improves the rotor performance significantly. When the speed rises to 280 km/h, the AoA of the retreating blade is already high enough when no dynamic twist is applied, although the influence law has not changed, the change in the value of AOA caused by the dynamic twist is small, and its improvement effect is not as great as at the speed of 230 km/h.

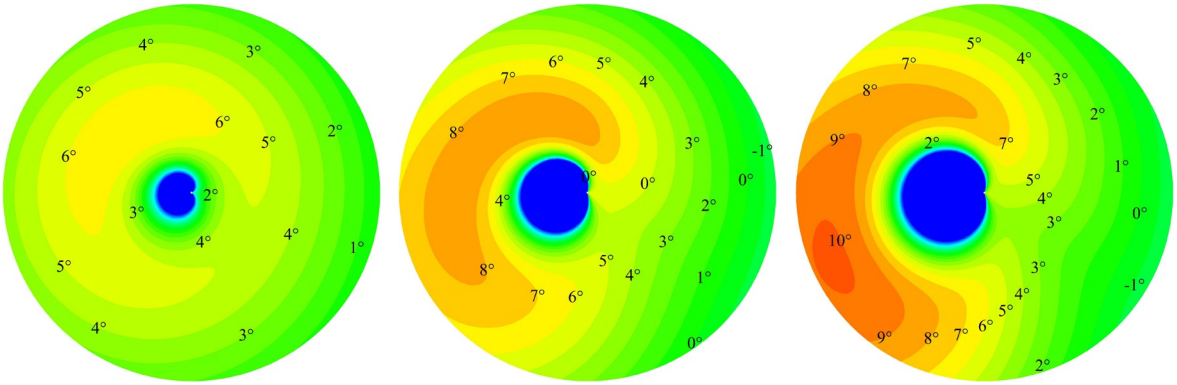

(a) 80 km/h (b) 230 km/h (c) 280 km/h

Figure 7 AoA distribution without dynamic twist

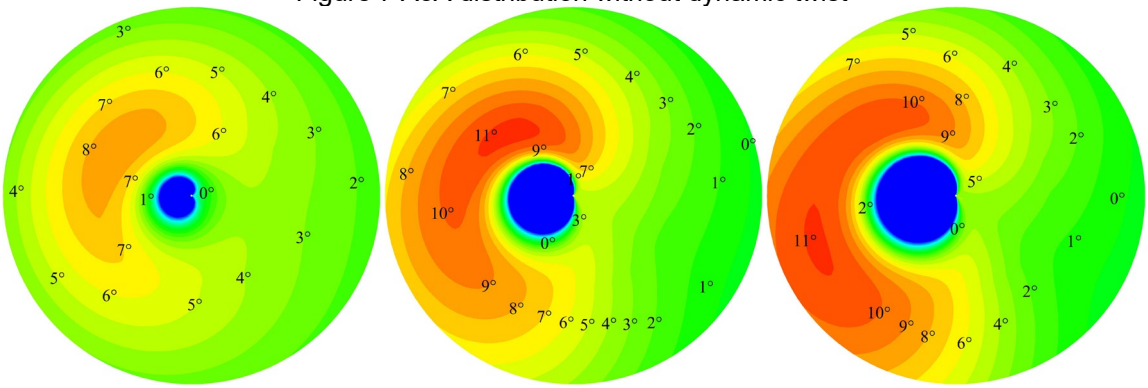

(a) 80 km/h (b) 230 km/h (c) 280 km/h

Figure 8 AoA distribution caused by dynamic twist ($\theta_{\mathrm{dt}}^{\mathrm{out}} = 5\ °/R, \phi_{\mathrm{dt}}^{\mathrm{out}} = 285°$)

4.2. Effect of Inner Segment Dynamic Twist

In this part, the effect of dynamic twist applied on the inner blade on rotor performance is studied. So there is no dynamic twist acting on the outer segment, which means that $\theta_{\mathrm{dt}}^{\mathrm{out}}$ in this part is set to 0.

4.2.1. View of the rotor power

Figure 9 shows the rotor power reduction while applying dynamic twist with different amplitudes and phase angles at a speed of 120 km/h on the inner segment. The influence law is similar to that of outer segment dynamic twist. A slight difference is that the best and worst phase angles become 330° and 150° respectively, which are about 30° different from the previous results.

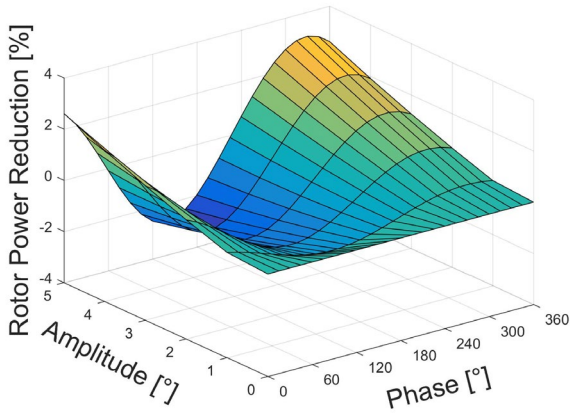

Figure 9 Power reductions with amplitude and phase

While the dynamic twist only acts on the inner blade, the dynamic twist angle θ_{dt} can be expressed as

$$\theta_{\mathrm{dt}} = \begin{cases} \frac{r}{R}\theta_{\mathrm{dt}}^{\mathrm{in}}\cos\left(N^{\mathrm{in}}\psi + \phi_{\mathrm{dt}}^{\mathrm{in}}\right) & \text{inner} \\ \frac{1}{2}\theta_{\mathrm{dt}}^{\mathrm{in}}\cos\left(N^{\mathrm{in}}\psi + \phi_{\mathrm{dt}}^{\mathrm{in}}\right) & \text{outer} \end{cases} \quad (36)$$

from Equation 35. It means that there is an equivalent dynamic twist on the outer blade with an amplitude of $\frac{1}{2}\theta_{\mathrm{dt}}^{\mathrm{in}}$ and a phase angle of $\phi_{\mathrm{dt}}^{\mathrm{in}}$.

4.2.2. View of AoA and L/D distribution

Figure 10 shows the difference in the L/D and AoA over the rotor disk caused by the dynamic twist on the inner blade compared with the case without the dynamic twist.

Because of the existence of the equivalent dynamic twist, the effect on the outer blade is similar to the case only outer segment dynamic twist acts. Compared with Figure 5(b), the L/D reduction in the middle of the retreating blade and increase at the tip of the advancing blade is less, while the reduction at the retreating blade tip becomes larger. For the inner segment, the dynamic twist causes a large decrease in the root of the advancing blade, which attenuates rapidly along the span direction.

In terms of AoA changes, the dynamic twist on the inner blade increases the AoA of the blade tip by about 0.3, and the AoA of the inner blade on the advancing side decreases to a certain extent. Compared with the case where dynamic twist acts only on the outer segment (Figure 6(b)), the AoA increase on the retreating side is reduced by a small amount, but also the area where the AoA reduction on the advancing side becomes smaller.

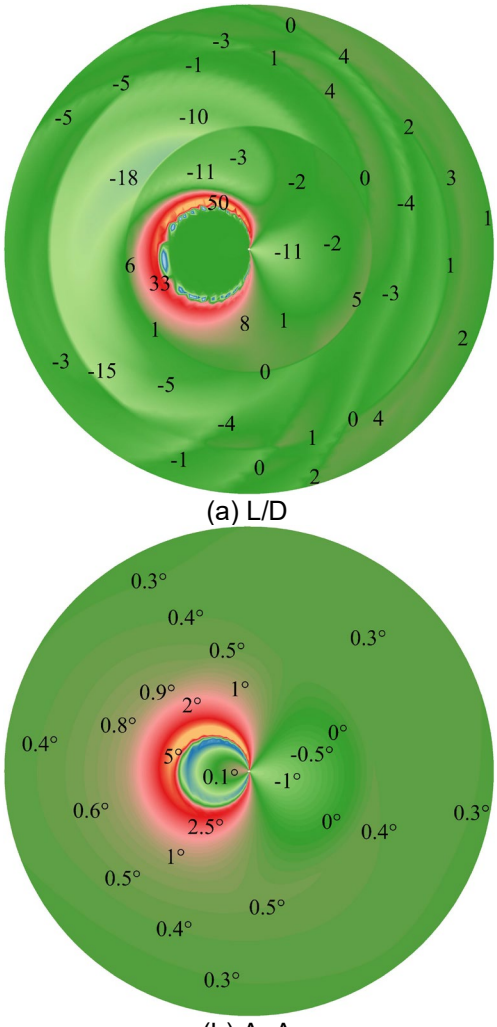

(a) L/D

(b) AoA

Figure 10 Difference caused by dynamic twist ($\theta_{\mathrm{dt}}^{\mathrm{out}} = 5\,°/R, \phi_{\mathrm{dt}}^{\mathrm{in}} = 285°, \mathrm{V} = 230\ \mathrm{km/h}$)

5. A PIECEWISE DYNAMIC TWIST SCHEME

Take rotor power as the design objective, the flight speed range is set to 0 – 300 km/h, the dynamic twist amplitude range of each segment is 0 – 5° /R, and the phase angle range is 0 – 360°. An optimal piecewise dynamic twist scheme is found by the traversal method, The amplitude of the scheme

for any speed is 5°/*R*, the phase angles of the scheme are shown in Figure 11.

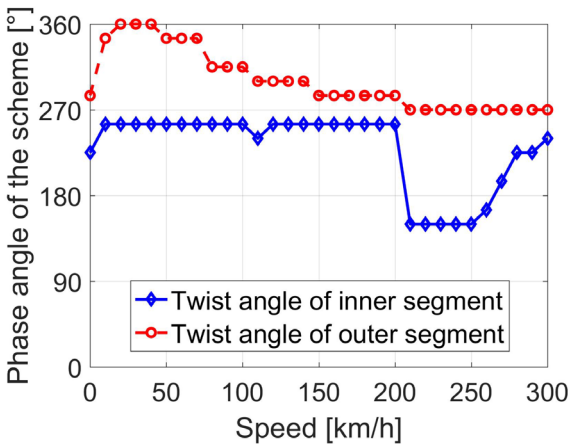

Figure 11 The optimal piecewise dynamic twist scheme

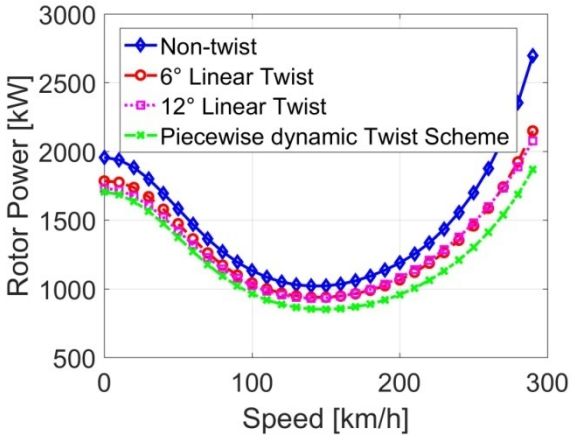

(a) Rotor power

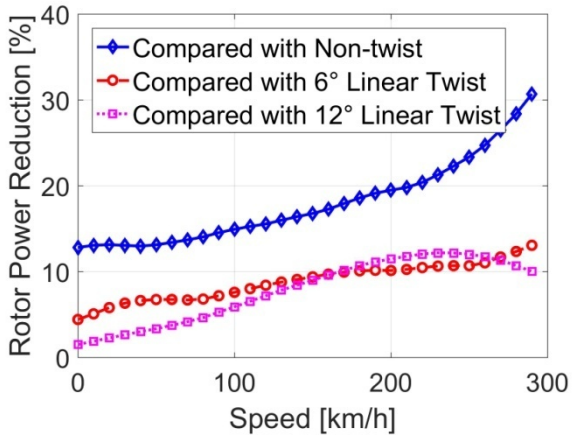

(b) Rotor power reduction

Figure 12 Rotor power and its reduction while applying piecewise dynamic twist

The rotor power and its reduction of the optimal scheme, non-twist, and the classic linear twist scheme are shown in Figure 12. The power with the optimal scheme is reduced by more than 10% at each flight speed compared with the case without the blade twist. Compared with the 6 °/*R* linear negative twist blade, the power is reduced by about 5% at hovering and maintains at about 10% after exceeding the speed of 160 km/h. Compared with the 12 °/*R* linear negative twist blade, the effect is average when hovering, gradually increases with the flight speed, and reaches 12.2% at 230 km/h.

6. CONCLUSIONS

This work focused on the investigation of the effects of dynamic twist acting on different segments of the rotor blade from the point of view of rotor performance. A calculation model including moderate deformation beam blade structure model, nonlinear quasi-steady aerodynamic model, Pitt-Peters inflow model, and trim model is established and used to analyze the rotor performance. The analysis yielded the following conclusions:

1) When the dynamic twist is applied to one segment, the rotor power reduction increases with its amplitude and changes periodically with the phase angle. If the phase angle is set to an appropriate value, the reduction first increases and then decreases with the flight speed.

2) If setting the phase angle to a proper value, the dynamic twist on the outer segment will increase the angle of attack at the advancing blade tip and the middle of the retreating blade, and reduces the angle of attack at the middle of the advancing blade. Except for the blade tip on the advancing side and the reverse flow area, the lift-to-drag ratio over the rotor disk is reduced to a certain extent, especially in the middle of the retreating blade.

3) If a dynamic twist is applied to the inner segment alone, there will be an equivalent dynamic twist acting on the outer segment. Most of the influence laws on the airflow environment are the same as the dynamic twist on the outer segment, but the value is smaller. In addition, the dynamic twist on the inner blade will slightly increase the angle of attack of the middle and tip part of the blade at all azimuth angles.

4) Through the optimal piecewise dynamic twist scheme, the rotor power can be reduced in the speed range of 0 – 300 km/h. Compared with the 6° linear negative twist scheme, the rotor power is reduced by more than 10%. Compared with the 12° linear negative twist scheme, the power is reduced by up to 12.2% at the speed of 230 km/h.

ACKNOWLEDGMENTS

This work is supported from the National Natural Science Foundation of China (11972181), the Open Research Foundation of the Key Rotor Aerodynamics Laboratory (2005RAL20200104) and

the Six Talent Peaks Project in Jiangsu Province (GDZB-013).

REFERENCES

[1] Gustafson, F. B., and Gessow, A., “Effect of Rotor-tip Speed on Helicopter Hovering Performance and Maximum Forward Speed,” NACA ARR L6A16, 1946.

[2] Gustafson, F. B., and Gessow, A., “Analysis of Flight-performance Measurements on a Twisted, Plywood-covered Helicopter Rotor in Various Flight Conditions,” NACA TN 1595, 1948.

[3] Gessow, A., “Flight Investigation of Effects of Rotor-blade Twist on Helicopter Performance in the High-Speed and Vertical-autorotative-descent Conditions,” NACA TR 1666, 1948.

[4] Shin, S., “Integral Twist Actuation of Helicopter Blades for Vibration Reduction,” Ph. D. Thesis, Massachusetts Institute of Technology, August, 2001.

[5] Wilbur, M. L., Mirick, P. H., William T. Yeager, J., Langston, C.W., Cesnik, C. E. S., and Shin, S., “Vibratory Loads Reduction Testing of the NASA/Army/MIT Active Twist Rotor,” American Helicopter Society 57th Annual Forum Proceedings, Washington, D.C., May 9-11 2001.

[6] Chen, P.C. and Chopra, I., “Hover Test of A Smart Rotor With Induced Strain Actuation Of Blade Twist”, AIAA Journal, Vol. 35, No. 1, January 1997, pp. 6-16.

[7] Rodgers, J.P. and Hagood, N.W., “Preliminary Mach-Scale Hover Testing of an Intergral Twist Actuated Rotor Blade”, SPIE’s Smart Structures and Materials Symposium, San Diego, March 1998.

[8] Chen, P.C. and Chopra, I., “Wind Tunnel Test Of A Smart Rotor Model With Individual Blade Twist Control”, Journal Of Intelligent Material Systems and Structures, Vol. 8, No. 5, May 1997, pp. 414-425.

[9] Cesnik, C.E.S and Shin, S., “On the Twist Performance of a Multiple Cell Active Helicopter Blade”, Smart Materials and Structures, Vol. 10, No. 1, February 2001, pp. 53-61.

[10] Q. Zhang, F. Hoffmann, B.G. “Van Der Wall, Benefit studies for rotor with active twist control using weak fluid–structure coupling”, 35th European Rotorcraft Forum, Hamburg, Germany, September 22–25, 2009.

[11] Wilkie, W.K., Park, K.C., and Belvin, W.K., “Helicopter Dynamic Stall Suppression Using Piezoelectric Active Fiber Composite Rotor Blades”, 39th AIAA Structures, Structural Dynamics, and Materials Conference, Long Beach, April 1998.

[12] Han D, V. Pastrikakis, and G. N. Barakos. “Helicopter flight performance improvement by dynamic blade twist.” Aerospace Science and Technology Vol. 58, 2016, pp. 445-452.

[13] D.D. Boyd Jr., “Initial aerodynamic and acoustic study of an active twist rotor using a loosely coupled CFD/CSD method”, 35th European Rotorcraft Forum, Hamburg, Germany, September 22–25, 2009.\

[14] Rohit J., “Examination of Rotor Loads due to On-Blade Active Controls for Performance Enhancement”, Journal of Aircraft, Vol. 47, No. 6, 2010, pp. 2049-2066.

[15] Harrison R, Stacey S, Hansford B. “BERP Ⅳ – the design, development and testing of an advanced rotor blade”, Proceedings of the 64th Annual Forum of AHS International, 2008, pp. 2524–2543.

[16] Paul W, Zincone R. “Advanced technology to the UH-60A and S-76 Helicopters”, Third European Rotorcraft and Powered Lift Aircraft Symposium, AIX-EN-PROVENCE, France, 1977.

[17] Zhang, X., et al. "Variable Twist Blade with Piecewise Linear Twist Control for Rotor Power Reduction", AIAA Scitech 2019 Forum, January 2019.

[18] Hodges D H, Dowell E H. “Nonlinear equations of motion for the elastic bending and torsion of twisted non-uniform blades: NASA-TN-D7818”, Washington, D. C., NASA, 1974.

[19] Hosges D H. “Nonlinear composite beam theory”. Virginia: the American Institute of Aeronautics and Astronautics, Inc., 2006, pp. 39-42.

[20] Peters D A, Haquang N. “Technical note: dynamic inflow for practical applications”, Journal of the American Helicopter Society, Vol. 33, No. 4, 1988, pp. 64-68.

[21] Owen D R J, Hinton E. “Finite elements in plasticity: theory and practice”, Swansea, U.K.: Pineridge Press, 1980, pp. 431-436.

[22] Yeo, H., Bousman, W.G. and Johnson, W., “Performance Analysis of a Utility Helicopter with Standard and Advanced Rotors,” Journal of the American Helicopter Society, Vol. 49, No. 3, 2004, pp. 250-270.